Improving Energy Transfer within Metal–Organic Frameworks by Aligning Linker Transition Dipoles along Framework Axis

Jierui Yu,[a] Ryther Anderson,[b] Xinlin Li, [a] Wenqian Xu,[c] Subhadip Goswami,[d] Sreehari Surendran Rajasree,[a] Karan Maindan, [a] Diego A. Gómez-Gualdrón,[b] and Pravas Deria*, [a]

[a] Department of Chemistry and Biochemistry, Southern Illinois University, 1245 Lincoln Drive, Carbondale, Illinois 62901, United States.

[b] Department of Chemical and Biological Engineering, Colorado School of Mines, 1500 Illinois St, Golden, Colorado 80401, United States.

[c] X-ray Science Division, Advanced Photon Source, Argonne National Laboratory, 9700 S Cass Ave, Lemont, Illinois 60439, United States.

[d] Department of Chemistry, Northwestern University, 2145 Sheridan Road, Evanston, Illinois 60208, United States.

KEYWORDS: Zr-MOF; MOF-photophysics; conjugated-linkers; exciton dynamics; anisotropic assembly.

ABSTRACT: Crystalline metal–organic frameworks (MOFs) can assemble chromophoric molecules into a wide range of spatial arrangements, which are controlled by the MOF topology. Like natural light-harvesting complexes (LHCs), the precise arrangement modulates interchromophoric interactions, in turn determining excitonic behavior and migration dynamics. To unveil the key factors that control efficient exciton displacements within MOFs, we first developed linkers with low electronic symmetry (as defined by large transition dipoles), and then assembled them into MOFs. These linkers possess extended conjugation along one molecular axis, engendering low optical bandgaps and improved oscillator strength for their lowest-energy transition ($S_0 \rightarrow S_1$). This enhances absorption-emission spectral overlap and boosts the efficiency of Förster resonance energy transfer, which was observed experimentally by a sizable decrease in emission quantum yield (QY), accompanied by a faster population decay profile. We find that MOFs that orient these elongated linkers along their asymmetric pore channel, *e.g.*, the hexagonal pores in a ***xly*** network, manifested >50% decrease in their emission QY with faster decay profiles relative to their corresponding solution dissolved linkers. This is due to an efficient migration of photo-generated excitons at the crystallite peripheral sites to internal sites, which was facilitated by polarized absorption-emission overlap among the parallelly aligned linkers. In contrast, symmetric MOFs, such as those with ***sqc-a*** topological net, orient elongated linkers along two perpendicular crystal axes, which hinder efficient exciton migration. The present study underscores that MOFs are promising to develop artificial LHCs, but that to achieve an efficient exciton displacement, appropriate topology-guided assembly is required to fully realize the true potential of linkers with low electronic symmetry.

INTRODUCTION

The elegant organization of photosynthetic pigments in natural light-harvesting complexes (LHC) has inspired chemists to design molecular assemblies that function with comparable efficiency.[1-8] Precise positioning of chlorophylls and other associated pigments in the rings of LH2 and LH1 gives rise to large spatial dispersion of the absorbed photon energy (defined by a delocalized exciton), ultrafast vectorial energy migration, and efficient delivery of this energy to a specific site (known as reaction center, RC) where energy is transduced into electrochemical potential energy. Achieving such functionalities in artificial chromophore assemblies has been difficult because it requires supramolecular assemblies that integrates chromophores in high (decimolar) concentrations, while maintaining long-range ordering. Such assembly would ensure large photon absorptivity and help overcome extant challenges stemming from various unproductive exciton recombination processes. Indeed, simple chromophore aggregates without a precise organization of their transition dipoles have not been found to manifest photosynthetic functionality.[9-17]

Intriguingly, crystalline metal–organic frameworks (MOFs),[18-26] which are constituted by inorganic nodes connected by organic linkers, provide a unique platform to engineer energy-transducing functionality similar to that of biological light-harvesting systems. By using functional, chromophoric molecules as linkers, these molecules could

adopt precise spatial organization as part of MOF crystals, which can be synthesized *via* well-established and scalable synthesis methods. The MOF ensembled chromophore arrangement differ from the simple chromophore aggregates as the molecular scale porosity of the MOF crystal ensures high photon absorptivity, dielectric modularity, and site accessibility. To this end, in recent experimental and theoretical work, we have established that chromophore assembly within MOFs gives rise to large spatial dispersion of the absorbed photon energy, producing molecular excitonic states.[27] Similar to those observed in natural LHCs, these excitonic states in MOFs feature a broad spectral envelope with significantly red-shifted transitions[27-30] and facilitate efficient energy transfer.[30-35] These findings suggests that improving energy transfer or exciton displacement within MOFs could define a crucial step in the future development of artificial LHCs. Here, we developed new MOF compositions to elucidate how the electronic structure of the chromophores impact exciton delocalization and migration, using a stepwise approach. First, we designed chromophoric linkers with low electronic symmetry (*e.g.* extended conjugation along one molecular axis). Second, we assembled the designed linkers into MOFs as to align their lowest energy transition dipoles along the same crystallographic axis.

In MOFs, excitation energy transfer occurs through self-exchange hopping process among the same type of chromophore molecules. Whilst the chromophore assembly works in a cohort, energy transfer in the singlet manifold can be analyzed (at least relatively) via the Förster resonance energy transfer (FRET) rate constant ($k_{FRET} = 2\pi J^2 \Theta/\hbar$), which depends on the the interchromophoric electronic coupling J (eV^{-1}), and the overlap integral Θ (eV^{-1}) between the area-normalized donor fluorescence and acceptor absorption bands.[31, 34, 36-38] J can be modulated by the MOF topology, as the latter defines the relative position and orientation of the chromophores.[31] While Θ can be primarily tuned by the design of the individual chromophore linkers. Since radiative decay from excited chromophores occurs through the lowest-energy state, *i.e.* $S_1 \rightarrow S_0$ transition, designing the linker as to boost the oscillator strength of the lowest energy vertical transition ($S_0 \rightarrow S_1$) should increase Θ.

Reticular chemistry has taught us that MOF topology is intimately tied to the symmetry of the constituent linkers. But MOF linkers are often highly symmetric, with π-conjugated aromatic cores, partly because these linkers are relatively easier to prepare and assemble into crystalline frameworks. However, due to degeneracy at their frontier molecular orbitals, these linkers typically present small transition dipoles for their respective lowest energy transitions. In contrast, chromophores with lower electronic symmetry manifest large *x*-polarized transition dipoles along their long-axis,[39] where the low electronic symmetry can be achieved by extending the π-conjugation along one molecular axis. Moreover, this strategy reduces the optical band gap, hence improving red (and near infrared) absorptivity. The challenge is then to organize chromophores with large *x*-polarized transition dipole in a way that they function in a cohort, where MOFs provide an opportunity to do so. Note that while simple molecular aggregates can organize these kinds of chromophores even in crystalline forms, this typically occurs in an alternative and perpendicular arrangements that do not fully leverage the large *x*-polarized transition dipole for light-harvesting functionality.

Therefore, in this work we aimed to demonstrate the synthesis of crystalline MOFs featuring anisotropic assemblies of chromophoric linkers with low electronic symmetry and study their potential to drive excitation energy migration efficiently. To this end, we investigated four linkers with triphenylene and phenylene-ethynylene backbones that align their lowest energy transition dipoles along their long molecular axis (**Chart 1**). We find that linkers with triphenylene core form frameworks with ***sqc-a*** topological nets (**Fig. 1**-top). For instance, the 5',5'''-bis(4-carboxyphenyl)-[1,1':3',1'':4'',1''':3''',1''''-quinquephenyl]-4,4''''-dicarboxylate (**PPP**) forms a known MOF, BUT-14.[40] Whereas the 5',5'''-bis(4-carboxyphenyl)-2'',5''-bis(trifluoromethyl)-[1,1':3',1'':4'',1''':3''',1''''-quinquephenyl]-4,4''''-dicarboxylate (**PPPF**) forms a new MOF, SIU-50, with isoreticular structure. Linkers with phenyl-ethynylene core, on the other hand, form anisotropic MOFs with ***xly*** nets (**Fig. 1**-bottom), which are an elongated variant of the ***csq*** net. The 5',5''''-(1,4-phenylenebis(ethyne-2,1-diyl))bis(([1,1':3',1''-terphenyl]-4,4''-dicarboxylate)) (**PEP**) provides the MOF SIU-75, and the 5',5''''-((2,5-bis(trifluoromethyl)-1,4-phenylene)bis(ethyne-2,1-diyl))bis(([1,1':3',1''-terphenyl]-4,4''-dicarboxylate)) (**PEPF**) gives rise to an isoreticular MOF, SIU-100.

Chart 1. Chemical Structures of Tetratropic Linkers with Low Electronically Symmetric

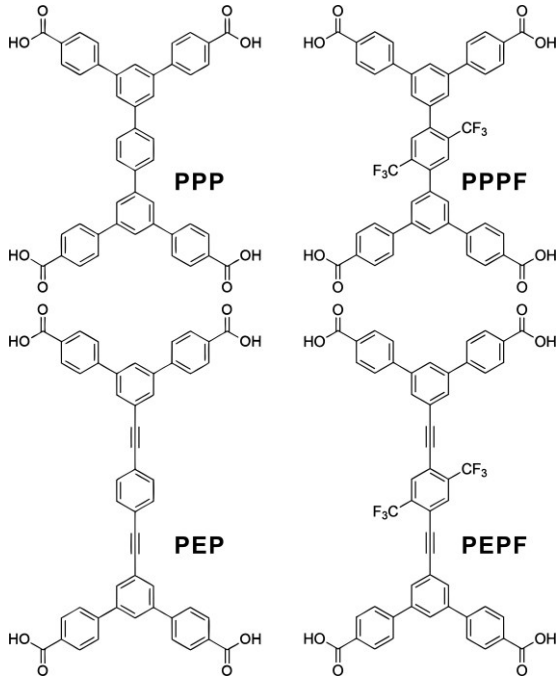

Steady-state and transient fluorescence spectroscopic data suggest that these linkers, which features large *x*-polarized transition dipoles, display a significant extent of emission and lifetime quenching when assembled in their respective frameworks due to efficient energy transfer. We expect, however, that the extent of quenching depends on

MOF topology. For instance, consider MOFs with ***xly*** nets, which have their chromophoric linkers aligned in such a way that all molecular transition dipoles are parallel to the *c*-axis of the crystallographic unit cell. This arrangement emphasizes an efficient energy transfer, facilitated by the parallel orientation of the absorptive and emissive dipole-oscillators. In contrast, the ***sqc-a*** topological net arranges the PPP (or PPPF) linkers into co-facial chains that run perpendicular to each other in alternative fashion. This arrangement does not align all the dipole oscillators along a unified direction, hence hindering the extent of energy transfer. Congruent with this picture, amplified emission quenching experiments with a post-synthetically installed, redox quencher indicated

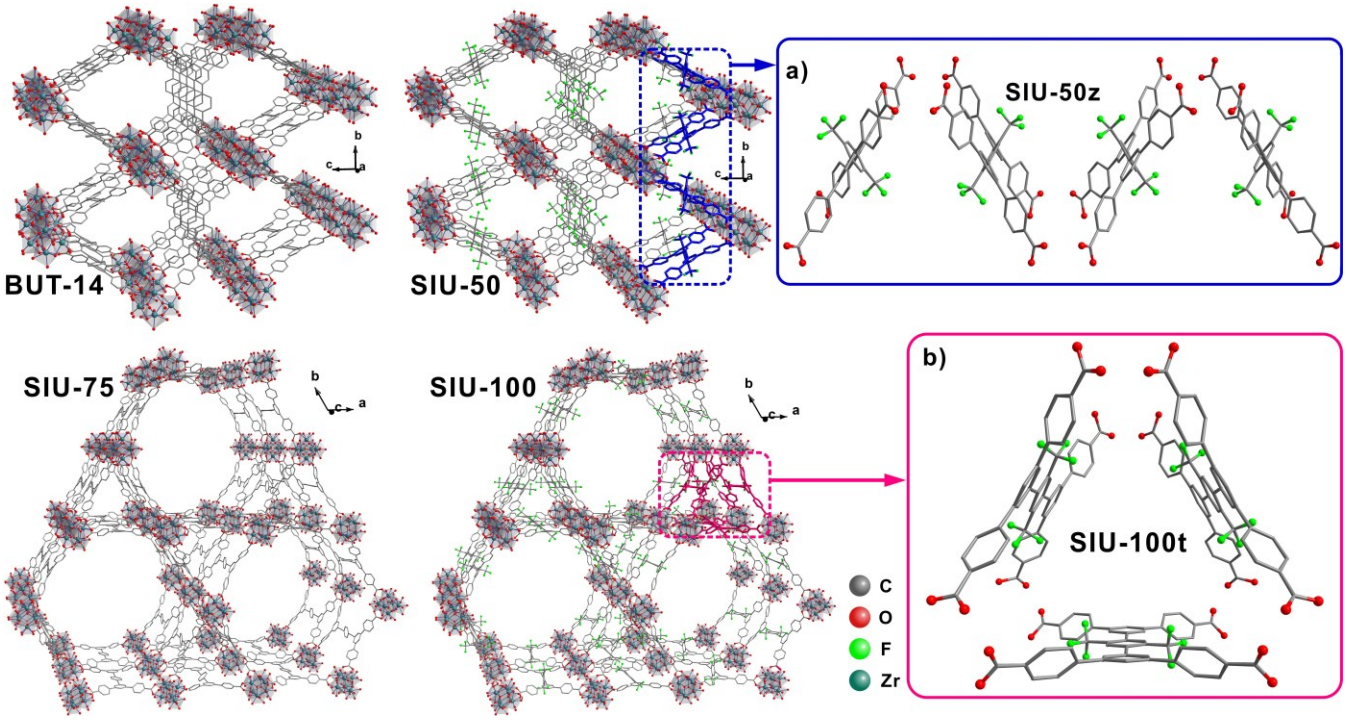

Figure 1. Structures of BUT-14, SIU-50, SIU-75 and SIU-100 MOFs. The right panels show the structures of small cluster models extracted from the MOF crystallographic cells: **a)** SIU-50z, **b)** SIU-100t. These models retained the crystallographic arrangement of the linkers in the MOFs and were used for TD-DFT calculations. Hydrogen atoms were omitted for clarity. See **Fig. S17** for further details.

that the perfect alignment of extended *x*-polarized transition dipoles enabled by the ***xly*** net is the superior assembly for efficient exciton energy transfer. The findings presented here could be translated into the future development of porous artificial light-harvesting systems with high exciton displacement efficiency, which is critically required to deliver these excitons into catalytic centers to convert into work producing charges.[41]

METHODS SECTION

Materials. All solvents used for spectroscopic studies, including 2-methyltetrahydrofuran (MeTHF), toluene (Tol), acetonitrile (MeCN) and α,α,α-trifluorotoluene (CF_3Tol), were purchased from Sigma-Aldrich and used as received. Details for linkers, MOF synthesis and relevant materials are presented in Supporting Information (SI Section **A**).

Instrumentation. Powder X-ray diffraction (PXRD) patterns were recorded with a Rigaku Ultima IV diffractometer (2θ scanned in the 2°- 20° range, with a 0.02° step at a 1.8°/min rate). Synchrotron powder diffraction data were collected at beamline 17-BM of the Advanced Photon Source at Argonne National Laboratory. Solvent (DMF)-soaked samples were loaded into Kapton capillaries (d= 1 mm). Diffraction data of these capillary-loaded samples were collected at the X-ray wavelength of 0.24153 Å using a VAREX XRD 4343CT flat panel detector. The obtained data was used for Rietveld refinement of computational MOF models to determine the experimental MOF structures (see SI section **C**). Scanning electron microscopy (SEM) images were collected using a Quanta FEG 450 SEM at 10kV. Nitrogen isotherms were recorded on Micromeritics ASAP 2020 analyzer at 77 K. Diffused reflectance spectra for MOF samples were measured using a JASCO V-670 UV-vis-NIR spectrophotometer that was equipped with a 60 mm $BaSO_4$–coated integrating sphere. Steady-state excitation-emission spectra and the fluorescence quantum-yields (QYs) were collected using an Edinburgh FS5 spectrofluorometer. These emission spectra were collected in a front-face configuration, where samples, soaked in the desired solvent, were packed in Teflon –sealed quartz capillary tube.[27, 41] Time-resolved emission decay profiles of the bulk sample were recorded using an Edinburgh Lifespec II Picosecond Time-Correlated Single-Photon Counting (TCSPC) spectrophotometer. The measurements were carried out with a 403 nm

pulsed diode laser (pulse width = 60 ps, providing 160 ps IRF) or a 310 nm pulsed LED (pulse width = 930 ps; providing 870 ps IRF) as the excitation light sources.

Computational Methods. Computational models for SIU-50, SIU-75 and SIU-100 were built using the publicly accessible code ToBaCCo-3.0.[42-43] The built models were optimized by minimizing the energy of the structure, where the dependence of energy on atom positions was provided by the Universal Force Field.[44] Then, the corresponding experimental PXRD patterns were used as the basis for Rietveld refinement (using Materials Studio-6.0)[45] of the models to elucidate the experimental lattice constants. Once these constants were found, atomic positions were reoptimized while keeping the lattice fixed. Slight adjustments of symmetry in the final MOF model were done "manually" using the Materials Studio-6.0 GUI.

The energy and oscillator strength of electronic excitations were computed on selected MOF-representative cluster models that were extracted from the crystallographic coordinates (**Fig. 1** and **Fig. S17**). In these calculations, the metal-oxo nodes were removed and a proton was added to each carboxylate group to achieve charge neutrality in the model.[27] The cluster models then underwent constrained optimization, where the terminal carboxylate moieties were fixed to their crystallographic coordinates, allowing the linkers to maintain their relative positions as defined by the respective framework topology. Oscillator strengths and their corresponding transition energies and densities were obtained *via* time-dependent density functional theory (TDDFT) using the HSEH1PBE functional and 6-311g(d, p) basis set (see details in SI section **E**). Calculations of 60 excited-states were performed on these DFT-optimized cluster models. TDM analyses were performed using the GPview software.[46]

RESULTS AND DISCUSSION

While chromophoric linkers with electronically symmetric conjugated cores are frequently used to construct a wide variety of MOFs, these linkers often display weak lowest-energy-transition ($S_0 \rightarrow S_1$) dipoles,[47] and thus small spectral overlap integral (Θ). Thus, our strategy to improve energy transfer in MOFs was underpinned by the design of linkers with extended conjugation along one molecular axis. This was accomplished by the introduction of tri-phenylene (PPP, PPPF) or phenylene-ethynylene (PEP, and PEPF) cores in tetratopic linkers (**Chart 1**). This design was exploited to break the degenerative nature of the frontier molecular orbitals, seeking to achieve long *x*-polarized transition dipoles (**Fig. S21**) and lower optical band-gaps.[48-54] Endowed with enhanced oscillator strength for their lowest-energy transitions (**Fig. S19**), these PPP/PEP-derived linkers are expected to display improved Θ (**Fig. S7**), thereby boosting the FRET process. However, it was presumed that an appropriate spatial arrangement was required for these chromophoric linkers to display any substantial light-harvesting functionality.

To investigate how the specific organization of these linkers impact their excitonic behavior and dynamics, we assembled the highly conjugated PEP and PEPF linkers into MOFs based on the asymmetric ***xly*** topological net. Respectively, SIU-75 (**Fig. 2**a) and SIU-100 (**Fig. 2**b)—SIU = Southern Illinois University. The ***xly*** topological net is one of the two extended topological variants (the other one being ***xlz***) derived from the well-established ***csq*** net. In ***xly*** nets, the longest axis of the linkers is aligned parallel to the *c*-axis of the crystallographic unit cell (see SI section **C1** discussion). For comparison, we also prepared MOFs that arrange linkers in alternative and perpendicular fashion as in ***sqc-a*** net. These frameworks are BUT-14 (**Fig. 2c**)[40] and SIU-50 (**Fig. 2d**). Note that three out of the four MOFs herein used to study energy transfer phenomena have been synthesized for the first time. The structures of these new MOFs (**Fig. 1**) were established *via* Rietveld refinement of MOF computational models against synchrotron diffraction data (see SI section **C**; **Fig. S11**, **S12**). Powder X-ray diffraction (PXRD) was used to determine the phase purity of the known BUT-14 sample (**Fig. S12a**).

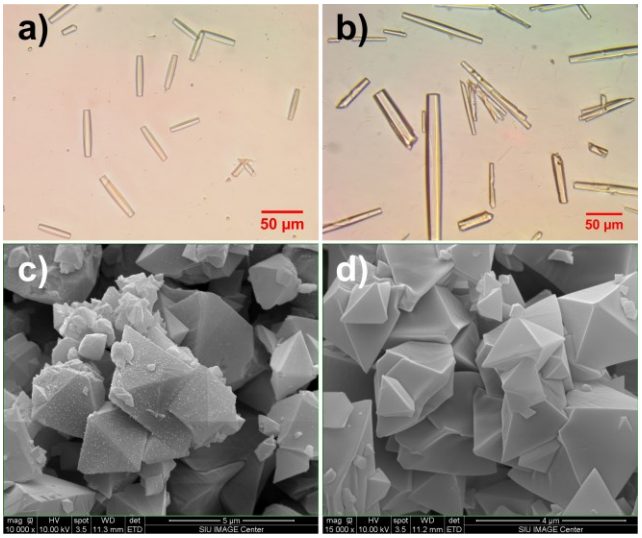

Figure 2. (**a, b**) Optical microscopic images for SIU-75 and SIU-100 showing anisotropic needle-shaped morphology, (**c, d**) SEM images for BUT-14 and SIU-50 showing symmetric octahedral crystallites.

Measured N_2 isotherms at 77 K suggests that, upon solvent removal, these MOFs undergo structural partial pore collapse on some regions of the material, which cannot be reversed exploiting the interactions between N_2 adsorbates and the framework. Although supercritical CO_2 activation (SCO) is often utilized to circumvent capillary-force-driven pore-shrinkage in MOFs, SCO seems ineffective for these MOFs. The extent of pore shrinkage seems to be less in MOFs constructed with $-CF_3$ derived linkers relative to the nonfunctionalized variant (**Fig. S13** and **S14**). That the pore collapse is limited to some regions of the materials is supported by the match between pore size distributions (PSDs) extracted from the corresponding N_2 isotherms of BUT-14 and SIU-50 and computationally predicted ones(see SI, Section D1; N_2 isotherms for SIU-75 and SIU-100 are not presented -they lost crystallinity upon solvent removal, *vide infra*).

Related framework "flexibility" is well-documented in MOFs. Particularly those with a long sidearms or "bendable"

cores,[55] as is the case for the elongated aromatic backbones used in our MOFs. Such structural changes can be seen in the PXRD patterns of the thermally activated SIU-75 and SIU-100 samples, which displayed broad envelopes with indistinguishable peak pattern, indicating the loss of crystallinity. The corresponding microscopic images display a heavily cracked crystal surface (**Fig. S15**). Thus, the synchrotron data was collected for DMF-filled MOF powders,[56] and porosity was determined from thermogravimetric analysis (TGA) of the samples. TGA showed significant mass loss associated with the loss of solvent initially filling the MOF pores (**Fig. S16**). The inferred solvent-accessible pore volumes matched well with the pore volumes for the corresponding crystallographic structures as predicted by PLATON 1.19.[57] BUT-14 showed 78.7 wt% loss (predicted as 77.5 vol%), SIU-50 underwent 76.4 wt% loss (predicted as 75.1 vol%), whereas SIU-75 and SIU-100 displayed 84.8 wt% (predicted 84.9 vol%) and 81.7 wt% (predicted 83.8 vol%) loss, respectively. For our spectroscopic investigations, MOF samples are soaked in a solvent and were never evacuated,[58] which warrants that measured properties corresponds to fully open structures, and thus calculations should focus on these framework configurations.

To understand how the variable extent of interchromophoric interactions among the chromophoric linkers defines unique excitonic properties in these frameworks,[28-29] we constructed a series of MOF-representative cluster models featuring small crystallographic segments of the linker assemblies. These non-exhaustive models are extracted from the crystallographic unit cell **Fig. 1**-right panel), so the chromophoric linkers in the clusters are positioned as they would be in the MOF crystal. In our calculation approach, we assume that the strongest interchromophoric interactions sufficiently define the electronic properties of the excited states representing the spectroscopic signature of the MOFs. Indeed, in our previous works, we established that the $[Zr_6(\mu_3\text{-}O)_4(\mu_3\text{-}OH)_4(-OH)_4(-OH_2)_4]^{8+}$ nodes are optoelectronically inert relative to conjugated aromatic linkers.[27, 30, 59-60] **Fig. 1** displays two such MOF-representative cluster models defining various cofacial geometries for **SIU-50** and **SIU-100** (see **Fig. S17** for the other two MOFs). The center-to-center distances in these conformations are 10.33 Å (in the **SIU-50z** model) and 10.79 Å (in the **SIU-100t** model).

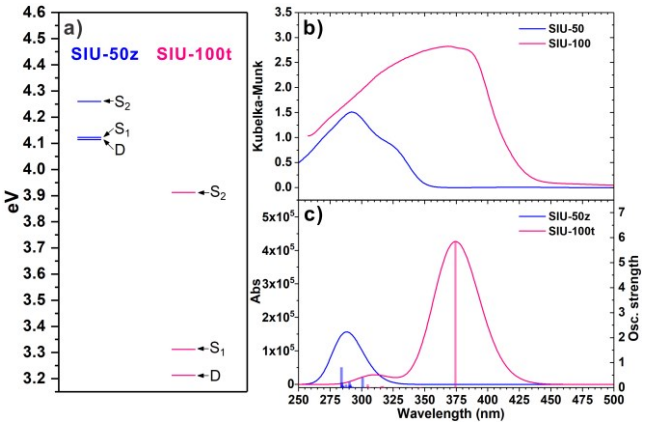

Figure 3. a) TDDFT–calculated energy levels for **SIU-50z** and **SIU-100t** models highlighting the lowest-energy bright and dark excited-states. **b)** Experimental diffuse reflectance spectra of the SIU-50 (*blue*) and SIU-100 (*pink*) MOF samples; **c)** TDDFT-calculated transition oscillator strengths and their corresponding absorptions spectra simulated (*via* gaussian reconvolution with fwhm = 0.37 eV) for the models presented in **Figure 1**.

TDDFT computed absorptive transition energies (**Fig. 3a** and **Fig. S20a**) and oscillator strengths reveal critical information regarding the evolution of excited states relative to the unassembled, solvated linker molecules. Experimental diffuse reflectance spectra of the MOF samples (**Fig. 3b** and **Fig. S18**) and UV-vis spectra of the solution-dissolved linkers (**Fig. S19**) match well with the TDDFT-predicted transitions. The experimental and computational data also suggest that the linkers with ethyne-connected cores (*i.e.* PEP, PEPF) possess higher oscillator strength for their respective lowest energy transitions than their corresponding directly connected variants (*i.e.* PPP and PPPF, **Fig. S19**).

Excitonic properties of the model compounds were examined by analyzing their respective transition density matrices (TDMs), which map atomistic electron-hole correlations during optical excitations. To achieve this, the linker atoms were systematically and consistently indexed (see **Fig. S17** for indexing scheme) before TDDFT computations. The matrix diagonal and off-diagonal densities represent excitonic wave function (center-of-mass) and the exciton size (distance between *e-h* particles), respectively.[17, 61-62] **Fig. 3a** summarizes the energies of various excited-states for **SIU-100t** and **SIU-50z** model compounds (see **Fig. S20a** for **SIU-75t** and **BUT-14z** models). The excited states were assigned by examining their energy, oscillator strength (for the respective vertical electronic excitations), and TDM (**Fig. 4**). Here, we focus mainly on the bright (optically allowed) S_1 states and the dark (optically forbidden) D states lying below them.

The TDM plots (**Fig. 4** and **Fig. S20b-e**) for the S_1 states show diagonal densities over all the linkers used in the models indicating that the excitonic wave functions are delocalized over all the PEP or PPP linker units. Besides the diagonal 'box-shaped' densities contributed by each linker, the non-zero off-diagonal densities (representing electron-hole, *e-h*, distances) for the S_1 states rapidly diminished with a residual density beyond one-linker units. These off-diagonal densities represent *e-h* correlation among the adjacent chromophores in the framework assembly, measuring a maximum exciton size of ~3.5 nm (extended over 3 units) for the ***scq-a*** MOFs **SIU-50** and **BUT-14**, and ~2.7 nm (3 units) for the ***xly*** MOFs **SIU-75** and **SIU-100**. Interestingly, the corresponding forbidden dark (D) states, lying below their bright S_1 states, also manifest similar TDMs. While the exact role of these dark states is yet to be fully established in MOFs, the similarity of their wavefunctions with the corresponding bright (S_1) states indicates that these D states may serve as a non-radiative exciton recombination route for S_1 state population, possibly reducing the overall emission QY of these MOF samples to some extent.

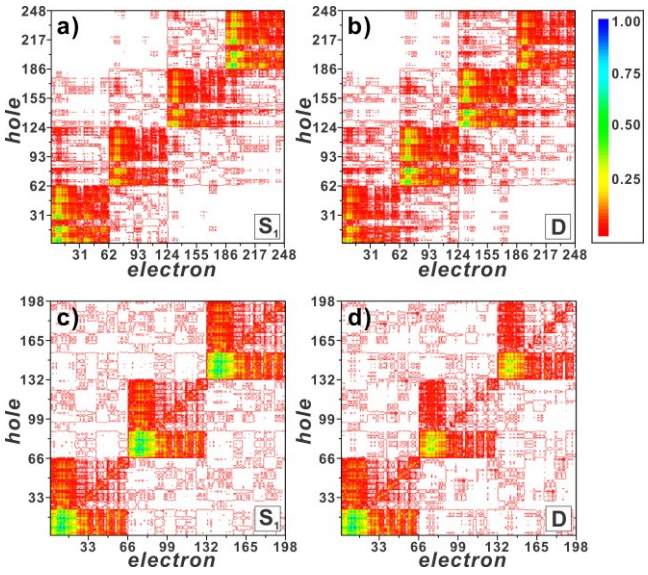

Figure 4. Contour plots of transition density matrices (TDMs) corresponding to optically relevant (**a, c**) bright (S_1) and (**b, d**) dark (D) first excited states (see **Fig. 3a** for their relative energies) for the cluster models (a, b) **SIU-50z** and (c, d) **SIU-100t**. These plots represent electron–hole correlation over each atom (the axes scales represent atom index) during an optical excitation. The color bar represents the normalized atomic transition densities.

The delocalized excitons in MOFs have a non-trivial impact on the extent of absorption-emission spectral overlap (Θ) compared to their solvated linkers. These include red-shifted electronic transitions with broader spectral envelopes relative to their free linkers (**Fig. 5**). This homogeneous line broadening is known to be a key feature in natural LHCs[63] resulting from the excited-states being shared by multiple chromophores. In our MOF samples, the contribution from inhomogeneous line-broadening stemming from crystal vibrations seems to be small. Specifically, the linewidth of the emission spectra collected over a range of 298-77K remained essentially unchanged (**Figure S9**). Nevertheless, an improved Θ in a MOF (**Figure 5**) boosts a FRET-like energy transfer process. Our data also highlights another interesting fact: the linkers with less-rigid core (*i.e.* without the -CF_3 groups) show slightly higher Θ relative to their rigid variants.

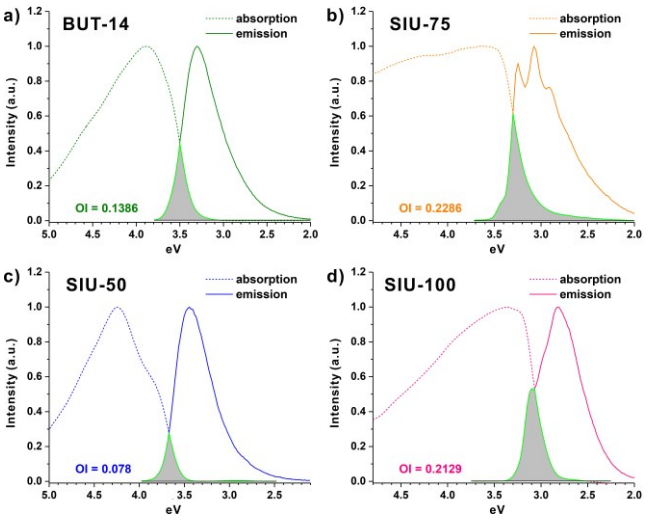

Figure 5. Frank-Condon mediated spectral overlaps (grey highlighted area) for the MOF samples with listed overlap integral Θ (in eV^{-1}) are also listed.

Since photo-generated excitons are initially created at the crystallite peripheral sites,[64] a rapid displacement of these excited populations, by an efficient FRET-like energy transfer process, to internal crystallite sites should result in a decrease in QY with faster population decay profile (reflected in respective emission lifetime).[65] Thus, the observed fluorescence QY and lifetime should depend upon the FRET efficiency defined by the linker symmetry and the topology of their arrangement.[66] We note that the D states (discussed above) may cause some non-radiative decay of the excited-state population, but they do not completely explain why the extent of diminished QY and lifetime would be topology-dependent. To gain a better understanding, we also examined the contribution of linker conformation (and rigidity) and various solvation parameters (*e.g.*, dispersity and acidity) on the QY and lifetimes for quenching in MOFs. **Fig. 6** summarizes the QY data for our four studied MOFs examined in MeTHF (δ_D = 17; acceptor number, AN = 8.0), CF_3Tol (δ_D = 17.5; AN = 14.9), and MeCN (δ_D = 15.3; AN = 18.9) media,[27] relative to their corresponding unassembled, solvated linkers. These data unambiguously suggest that the ***xly*** MOFs (*i.e.* **SIU-75** and **SIU-100**) constructed from more extensively conjugated ethynyl-phenyl linkers record a large decrease in QY (>50%) relative to their respective linkers. In contrast, relatively symmetric ***sqc-a*** MOFs (*i.e.*, **BUT-14** and **SIU-50**) suffer only a nominal (<30%) decrease in QY relative to their respective linkers. Furthermore, MOFs with the CF_3-bearing linkers display less pronounced decrease in QY compared to their non-CF_3 variants. Consider that for SIU-100 and SIU-50 (constructed from PEPF and PPPF linkers with CF_3-phenylene as their central core) show 53% and 22% QY decrease, whereas SIU-75 and BUT-14 report 63% and 29% decrease in QY, respectively. While both trend parallel with their corresponding Θ (**Fig. 6**; *vide supra*), the conformational limitation or rigidity imparted by the CF_3-phenylene cores seems to be a reason for higher QY relative to their less-rigid analogs. Additionally, the QY data summarized in **Fig. 6** suggests a solvent dependency. In general, MOFs with CF_3-phenylene linkers (PPPF, and PEPF), in both

the ***xly*** and ***sqc-a*** topological nets, show higher QY in an acidic solvent like CF_3Tol and lower in MeTHF solvents. In contrast, MOFs with comparatively electron-rich PPP and PEP cores display a reverse order, *i.e.* a higher QY observed in MeTHF solvent. Interestingly, all MOF samples filled with MeCN solvent rendered a low QY, possibly due to a low solvent dispersity (δ_D = 15.3)[27] that allows a lower extent of solvent-MOF interaction. Thus, the impact of solvent in the measured photophysical properties is not large and mainly defined by the electronic nature of the MOF surface and the extent by which it interacts with solvent molecules.[27]

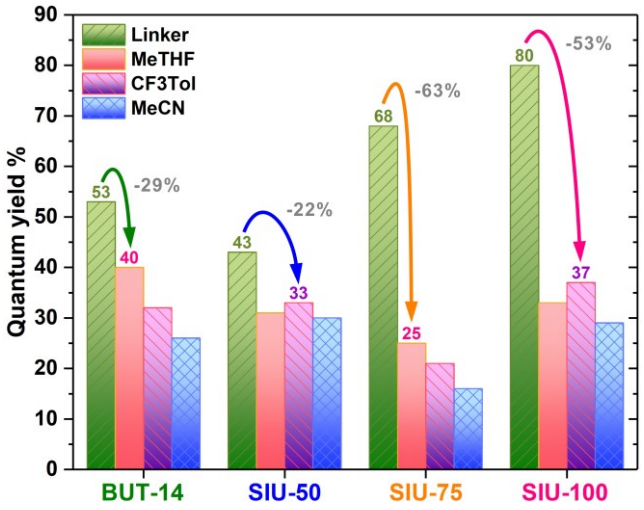

Figure 6. Fluorescence QY measured for the MOF samples in three different solvents relative to their corresponding solvated linkers (*green*; *ca* 30 μM in DMF solvent). The measured difference in QY values is noted in *grey*.

Transient fluorescence decay profiles of the MOF samples were examined against their respective linkers to determine the relative depletion of the emission population. **Fig. 7** highlights the transient profiles for BUT-14, SIU-50, and SIU-100 MOFs along with their solubilized PPP, PPPF, and PEPF linkers in DMF solvent. The corresponding lifetime data are summarized in **Table 1**. These data were recorded in a solvent that rendered the highest emission QY for the respective MOFs[67] as to avoid any possible solvent-mediated quenching process during the comparison. Consistent with the trend observed for the steady-state emission, the transient profiles clearly show that MOFs with large Θ values, and displayed more decrease in QY, manifest a steeper lifetime profile (*i.e.* large extent of lifetime quenching) relative to their respective linkers. For example, SIU-100 shows a two-component decay profile with τ_1 = 0.89 ns (85%) as a major process, whereas the corresponding free PEPF linker possesses a single component (τ = 3.2 ns) decay profile. In contrast, SIU-50 shows nominal self-quenching represented by a two-component decay profile with τ_1 = 3.2 ns (31%) and τ_2 = 8.9 ns (69%), with the corresponding PPPF linker reporting a single component decay (τ = 9.2 ns). BUT-14 also rendered similar trend with τ_1 = 3.1 ns (32%) and τ_2 = 12.8 ns (68%), compared to its PPP linker with single component decay constant of 12 ns. The PEP linker that forms SIU-75 shows a significantly high radiative rate with a fast, single component decay (*ca* 0.69 ns; **Fig. S10**). This time-constant is shorter than the 0.869 ns IRF with our 310 nm pulsed LED excitation source, therefore any faster decay in SIU-75 MOF sample could not be well-resolved.

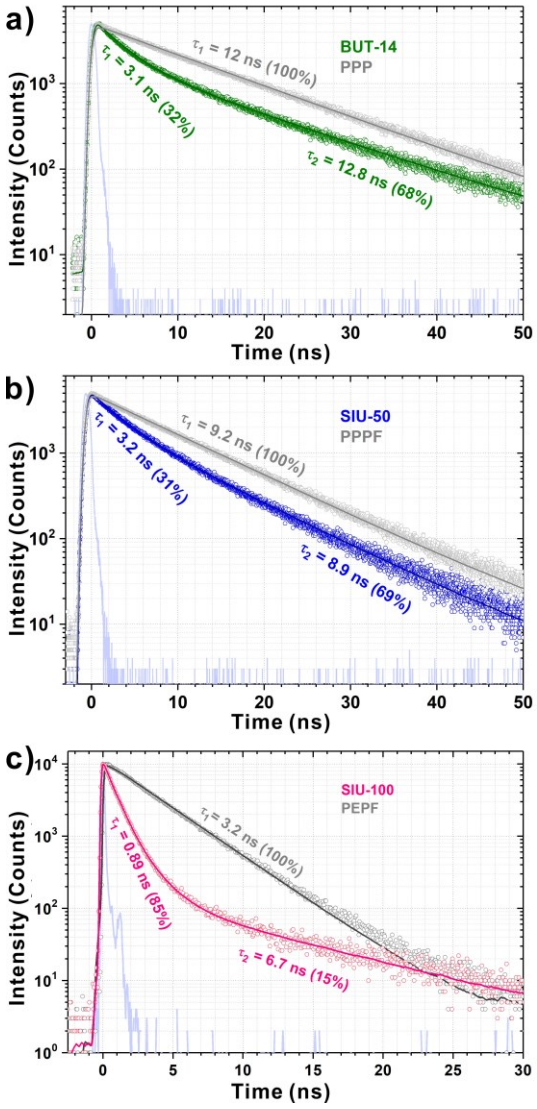

Figure 7. Transient fluorescence decay profiles for the MOFs plotted against their respective linkers (grey profile): **a)** BUT-14 and PPP, **b)** SIU-50 and PPPF, and **c)** SIU-100 and PEPF. For the MOF samples, the experiments were carried out in solvents that provided the highest QY. Experimental condition: BUT-14: λ_{ex} = 310 nm, MeTHF; SIU-50: λ_{ex} = 310 nm, CF_3Tol; SIU-100: λ_{ex} = 405 nm, CF_3Tol. The time constants are presented in **Table 1**.

Table 1. QY and Emission Time-Constants of the MOF Samples Relative to Their Corresponding Free Linkers

Compound	QY (%)	τ_1 (ns)	τ_2 (ns)
PPP	53 [c]	12 (100%)	
BUT-14	38 [a]	3.1 (32%)	12.8 (68%)
PPPF	43 [c]	9.2 (100%)	

SIU-50	33 [b]	3.2 (31%)	8.9 (69%)
PEP	68 [c]	0.69 (100%)	
SIU-75	25 [a]	-	-
PEPF	80 [c]	3.2 (100%)	
SIU-100	37 [b]	0.9 (85%)	6.7 (15 %)

[a] MeTHF, [b] CF_3-Tol, [c] DMF solvent.

Coming back to Θ, all computational and experimental data suggest that the ethynylene-elaborated linkers display higher QY and larger $S_0 \leftrightarrow S_1$ Frank-Condon-mediated overlap in their unassembled solvated form. However, when these highly radiative linkers are assembled in MOF crystals, a large emissive population becomes invisible to the detector—the underlying mechanism seems to be efficient, at least, faster than their lifetime. Given that there is no redox quencher present in these MOFs, only an efficient FRET-like energy transfer process can lead to such quenching by displacing the exciton population within the interior of the crystals. In this regard, the ***xly*** topological net orients all the linkers along its *c*-axis, which facilitates an extremely facile exciton displacement through a polarized absorption-emission overlap.[68] In contrast, the ***sqc-a*** net (SIU-50, BUT-14) orients the linker's transition dipoles along two perpendicular axes (**Figure 1**), thus significantly limiting the efficiency of exciton migration through absorption-emission overlap. This reasoning is supported by the anisotropic emission of ***xly*** MOF studied here: SIU-100 manifest an emission anisotropy of 0.8 which was maintained above 0.6 for its entire lifetime (> 6 ns).

The efficiency of the FRET-like process within these topologically different MOFs was finally probed *via* amplified emission quenching experiments involving a redox quencher. In this experiment, the quencher is typically installed near the chromophoric linker such that a facile exciton hopping would dramatically enhance the quenching perimeter of this quencher. Since our MOFs are constructed from an unsaturated 8-connected Zr_6-oxo node, they were exploited to install carboxy-terminated redox species (a common Zr_6-oxo node, like those used here, can have a maximum of 12-carboxylates). Ferrocene carboxylate was installed as redox quencher[69] at the node using a well-established solvent assisted ligand incorporation (SALI, see SI section **F**) with varying Fc/linker ratio.[28, 30, 69-71] These Fc-decorated MOF samples show a monotonous decrease in the emission intensity with increase in Fc-loading –the relation can be analyzed using Stern-Volmer relationship:

$$\frac{I_0}{I_s} = \frac{Q_0}{Q_s} = 1 + K_{SV}[R] \qquad \text{(Eq 1)}$$

Here, Q_0 and Q_s are the intrinsic (*i.e.*, without quencher) QY and saturated QY and I_0 and I_s are respective emission intensity, and $[R]$ is redox quencher doping ratio with respect to the linker (determined by SEM-EDS elemental analysis). Since the Fc-quencher is fixed at the Zr-oxo node - close to the linkers, the emission quenching will not follow a standard diffusion-controlled mechanism –rather, a quenching process where K_{SV} would relate to the number of linkers the exciton visits within its lifetime.[28, 31, 69] The analysis of the quenching data (**Figure 8**) revealed that the K_{SV} values for ***scq-a*** MOFs (96 for BUT-14 and 85 for SIU-50) are generally lower compared to ***xly*** MOFs (169 for SIU-75 and 150 for SIU-100). These data unambiguously indicate that the ***xly*** MOF facilitates approximately double the number of sites that an exciton can visit compared to that in a ***sqc-a*** framework. Considering their respective lifetimes, the rate of energy transfer can be estimated as *ca* 1.3 ps for BUT-14, 1.7 ps for SIU-50, and 0.16 ps for SIU-100.

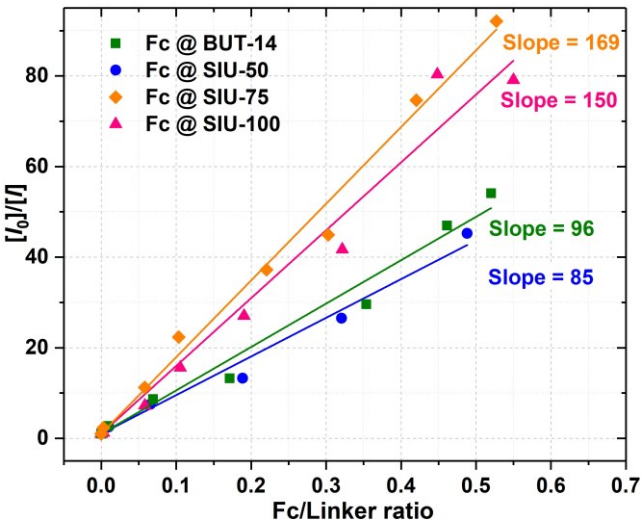

Figure 8. The Stern-Volmer plot of BUT-14 (*olive*), SIU-50 (*blue*), SIU-75 (*orange*), and SIU-100 (*pink*) with node-installed ferrocenecarboxylate as the redox quencher.

CONCLUSIONS

In this study we have developed a two-step strategy to improve the exciton-energy transfer within metal–organic frameworks. First, linkers with expanded conjugation along one molecular axis were developed; second, these elaborated chromophoric linkers were assembled into MOFs as to align in anisotropic fashion *via* reticular chemistry. Four linkers with varying conjugation length and side-chain functionality were prepared: direct phenyl-phenyl connectivity provided PPP and PPPF linkers, whereas ethynylene connected phenyl generated PEP and PEPF variants. Expanding the conjugation along one molecular axis lowers the electronic symmetry of the linkers engendering a smaller optical bandgap. This resulted in red-shifted electronic transition with large *x*-polarized transition dipole (along the molecular axis) for their lowest-energy transition. A corollary is that these linkers are featured with high absorption-emission spectral overlap defined by large overlap integral, Θ, which will lead to improve FRET-like energy transfer processes. Conformational flexibility and electronic properties of a given chromophore core were modulated with two $-CF_3$ groups at the central phenyl ring of the PPPF and PEPF linkers. To investigate how the specific organization of these linkers impact their excitonic behavior and dynamics, all four linkers were assembled in two different topological nets constructed from 8-connected Zr-oxo nodes. The highly conjugated PEP and PEPF linkers into SIU-75 and SIU-100, respectively, based on the asymmetric ***xly*** topolog-

ical net. For comparison, we also prepared MOFs that arrange linkers in alternative and perpendicular fashion as in ***sqc-a*** net. These are BUT-14 and SIU-50, respectively, from PPP and PPPF linkers.

The computational and experimental data underscore that the ethynylene-elaborated linkers possess large $S_0 \rightarrow S_1$ Frank-Condon mediated overlap and display higher QY in their solvated form. However, when these extended linkers were assembled in MOF crystals, a significant emissive excited-state population became undetectable. For example, the PEP and PEPF derived SIU-75 and SIU-100 displayed >50% decrease in QY with a steeper decay profile relative to their respective linkers. Rapid displacement of the photogenerated excitons from the exterior sites, where they were initially created, to the internal crystallite sites indicates efficient energy transfer through a FRET like process. Since a ***xly*** framework (SIU-75, SIU-100) arranges all its chromophoric linkers along their *c*-axis, parallelly oriented *x*-polarized transition dipoles trigger an efficient exciton displacement through large absorption-emission overlap involving in-phase oscillators. In contrast, the symmetric ***sqc-a*** net (SIU-50, BUT-14) orients the linker's transition dipoles along two perpendicular axes, which hinders efficient exciton migration. The linkers with the $-CF_3$ groups at their central phenyl ring were restricted in rotational flexibility, which is sufficient to manifest smaller Θ and therefore, the respective MOFs displayed less pronounced decrease in QY relative to their non-functionalized analogs.

Amplified redox quenching experiments, mediated by node anchored ferrocene moieties, unambiguously verify that the ***xly***-MOFs (SIU-75 and SIU-100) are the superior assembly for excitation energy transfer compared to those in ***sqc-a*** networks. The four chromophoric linkers and their respective MOFs studied here have manifested Θ ranged from 0.08 - 0.23 eV^{-1}. Even within the realm of this small range, we have demonstrated that extending molecular conjugation can be a viable way to improve low-energy transition oscillator strength and the Θ, but that to achieve an efficient exciton displacement, appropriate topology-guided assembly is required to fully realize the true potential of linkers with low electronic symmetry. Study with chromophoric linkers that would provide larger Θ value can be a subject of future development.

ASSOCIATED CONTENT

Supporting Information. Synthetic details, computational and spectroscopic data. This material is available free of charge at http://pubs.acs.org.

AUTHOR INFORMATION

Corresponding Author

* Pravas Deria
pderia@siu.edu.

ORCID

Jierui Yu: 0000-0001-8422-3583
Ryther Anderson: 0000-0001-8985-0471
Xinlin Li: 0000-0002-9106-5250
Wenqian Xu: 0000-0002-4815-6253
Subhadip Goswami: 0000-0002-8462-9054
Karan Maindan: 0000-0001-7252-7328
Diego A. Gómez-Gualdrón: 0000-0003-3237-0199
Pravas Deria: 0000-0001-7998-4492

Author Contributions

All authors have approved the final version of the manuscript.

ACKNOWLEDGMENT

P.D. gratefully acknowledges funding from the National Science Foundation (NSF CAREER CHE-1944903). J.Y. acknowledges the B. & M. Gower fellowship awarded through the Department of Chemistry and Biochemistry, and dissertation research award through graduate school, SIUC. D.A.G.-G. thanks support from NSF CAREER Award (CBET 1846707). SEM data were collected at SIUC IMAGE center (supported by NSF grant CHE-0959568). This research used Beamline 17-BM of the Advanced Photon Source, a U.S. Department of Energy (DOE) Office of Science User Facility operated for the DOE Office of Science by Argonne National Laboratory under Contract No. DE-AC02-06CH11357. We also thank Edinburgh Instruments, Ltd. for the generous loan of EPLED 310 nm pulsed LED laser to complete the TCSPC measurements.

REFERENCES

1. Gray, H. B., Powering The Planet With Solar Fuel. *Nat. Chem.* **2009,** *1*, 7.
2. Leem, G.; Sherman, B. D.; Burnett, A. J.; Morseth, Z. A.; Wee, K.-R.; Papanikolas, J. M.; Meyer, T. J.; Schanze, K. S., Light-Driven Water Oxidation Using Polyelectrolyte Layer-by-Layer Chromophore–Catalyst Assemblies. *ACS Energy Lett.* **2016,** *1*, 339-343.
3. Mulfort, K. L.; Utschig, L. M., Modular Homogeneous Chromophore–Catalyst Assemblies. *Acc. Chem. Res.* **2016,** *49*, 835-843.
4. Kohler, L.; Mulfort, K. L., Photoinduced electron transfer kinetics of linked Ru-Co photocatalyst dyads. *J. Photochem. Photobiol. A* **2019,** *373*, 59-65.
5. Swierk, J. R.; Mallouk, T. E., Design and Development of Photoanodes for Water-Splitting Dye-Sensitized Photoelectrochemical Cells. *Chem. Soc. Rev.* **2013,** *42*, 2357-2387.
6. Lebedeva, N. V.; Schmidt, R. D.; Concepcion, J. J.; Brennaman, M. K.; Stanton, I. N.; Therien, M. J.; Meyer, T. J.; Forbes, M. D. E., Structural and pH Dependence of Excited State PCET Reactions Involving Reductive Quenching of the MLCT Excited State of $[Ru^{II}(bpy)_2(bpz)]^{2+}$ by Hydroquinones. *J. Phys. Chem. A* **2011,** *115*, 3346-3356.
7. Khnayzer, R. S.; Blumhoff, J.; Harrington, J. A.; Deng, F.; Haefele, A.; Castellano, F. N., Upconversion-Powered Photoelectrochemistry. *Chem. Commun.* **2012,** *48*, 209-211.
8. O'Regan, B.; Grätzel, M., A Low Cost, High-Efficiency Solar Cell Based on Dye-Sensitized Colloidal TiO2 Films. *Nature* **1991,** *353*, 737-740.
9. Williams, D. E.; Dolgopolova, E. A.; Pellechia, P. J.; Palukoshka, A.; Wilson, T. J.; Tan, R.; Maier, J. M.; Tan, R.; Greytak, A. B.; Smith, M. D.; Krause, J. A.; Shustova, N. B., A Mimic of the Green Fluorescent Protein β-barrel: Photophysics and Dynamics of Confined Chromophores Defined by a Rigid Porous Scaffold. *J. Am. Chem. Soc.* **2015,** *137*, 2223-2226.
10. Williams, D. E.; Martin, C. R.; Dolgopolova, E. A.; Swifton, A.; Godfrey, D. C.; Ejegbavwo, O. A.; Pellechia, P. J.; Smith, M. D.; Shustova, N. B., Flipping the Switch: Fast Photoisomerization in a Confined Environment. *J. Am. Chem. Soc.* **2018,** *140*, 7611-7622.
11. Scholes, G. D.; Rumbles, G., Excitons in Nanoscale Systems. *Nat. Mater.* **2006,** *5*, 683–696.

12. Lim, S.-H.; Bjorklund, T. G.; Spano, F. C.; Bardeen, C. J., Exciton Delocalization and Superradiance in Tetracene Thin Films and Nanoaggregates. *Phys. Rev. Lett.* **2004,** *92*, 107402.

13. Scholes, G. D.; Fleming, G. R.; Olaya-Castro, A.; Grondelle, R. v., Lessons from Nature about Solar Light Harvesting. *Nat. Chem.* **2011,** *3*, 763-774.

14. Silva, D. L.; Murugan, N. A.; Kongsted, J.; Ågren, H.; Canuto, S., Self-Aggregation and Optical Absorption of Stilbazolium Merocyanine in Chloroform. *J. Phys. Chem. B* **2014,** *118*, 1715-1725.

15. Stork, M.; Gaylord, B. S.; Heeger, A. J.; Bazan, G. C., Energy Transfer in Mixtures of Water-Soluble Oligomers: Effect of Charge, Aggregation, and Surfactant Complexation. *Adv. Mater.* **2002,** *14*, 361-366.

16. Liu, Y. H.; Zhao, J. B.; Li, Z. K.; Mu, C.; Ma, W.; Hu, H. W.; Jiang, K.; Lin, H. R.; Ade, H.; Yan, H., Aggregation and Morphology Control Enables Multiple Cases of High-Efficiency Polymer Solar Cells. *Nat. Commun.* **2014,** *5*, 5293.

17. Tretiak, S.; Mukamel, S., Density Matrix Analysis and Simulation Of Electronic Excitations in Conjugated and Aggregated Molecules. *Chem. Rev* **2002,** *102*, 3171-3212.

18. Eddaoudi, M.; Kim, J.; Rosi, N.; Vodak, D.; Wachter, J.; O'Keeffe, M.; Yaghi, O. M., Systematic Design of Pore Size and Functionality in Isoreticular MOFs and Their Application in Methane Storage. *Science* **2002,** *295*, 469-472.

19. Furukawa, H.; Cordova, K. E.; O'Keeffe, M.; Yaghi, O. M., The Chemistry and Applications of Metal-Organic Frameworks. *Science* **2013,** *341*, 1230444.

20. Yaghi, O. M.; O'Keeffe, M.; Ockwig, N. W.; Chae, H. K.; Eddaoudi, M.; Kim, J., Reticular Synthesis and the Design of New Materials. *Nature* **2003,** *423*, 705-714.

21. Horike, S.; Shimomura, S.; Kitagawa, S., Soft Porous Crystals. *Nat. Chem.* **2009,** *1*, 695-704.

22. Kitagawa, S.; Kitaura, R.; Noro, S.-i., Functional Porous Coordination Polymers. *Angew. Chem. Int. Edit.* **2004,** *43*, 2334-2375.

23. Kitaura, R.; Seki, K.; Akiyama, G.; Kitagawa, S., Porous coordination-polymer crystals with gated channels specific for supercritical gases. *Angew. Chem. Int. Edit.* **2003,** *42*, 428-431.

24. Férey, G., Hybrid Porous Solids: Past, Present, Future. *Chem. Soc. Rev.* **2008,** *37*, 191-214.

25. Férey, G.; Mellot-Draznieks, C.; Serre, C.; Millange, F.; Dutour, J.; Surblé, S.; Margiolaki, I., A Chromium Terephthalate-Based Solid with Unusually Large Pore Volumes and Surface Area. *Science* **2005,** *309*, 2040-2042.

26. Farha, O. K.; Yazaydın, A. Ö.; Eryazici, I.; Malliakas, C. D.; Hauser, B. G.; Kanatzidis, M. G.; Nguyen, S. T.; Snurr, R. Q.; Hupp, J. T., *De novo* Synthesis of a Metal–Organic Framework Material Featuring Ultrahigh Surface Area and Gas Storage Capacities. *Nat. Chem.* **2010,** *2*, 944-948.

27. Yu, J.; Park, J.; Van Wyk, A.; Rumbles, G.; Deria, P., Excited-State Electronic Properties in Zr-Based Metal-Organic Frameworks as a Function of a Topological Network. *J. Am. Chem. Soc.* **2018,** *140*, 10488-10496.

28. Deria, P.; Yu, J.; Balaraman, R. P.; Mashni, J.; White, S. N., Topology-Dependent Emissive Properties of Zirconium-Based Porphyrin MOFs. *Chem. Commun.* **2016,** *52*, 13031-13034.

29. Deria, P.; Yu, J.; Smith, T.; Balaraman, R. P., Ground-State versus Excited-State Interchromophoric Interaction: Topology Dependent Excimer Contribution in Metal–Organic Framework Photophysics. *J. Am. Chem. Soc.* **2017,** *139*, 5973-5983.

30. Yu, J.; Li, X.; Deria, P., Light-Harvesting in Porous Crystalline Compositions: Where We Stand toward Robust Metal-Organic Frameworks. *ACS Sustainable Chem. Eng.* **2019,** *7*, 1841-1854.

31. Son, H.-J.; Jin, S.; Patwardhan, S.; Wezenberg, S. J.; Jeong, N. C.; So, M.; Wilmer, C. E.; Sarjeant, A. A.; Schatz, G. C.; Snurr, R. Q.; Farha, O. K.; Wiederrecht, G. P.; Hupp, J. T., Light-Harvesting and Ultrafast Energy Migration in Porphyrin-Based Metal–Organic Frameworks. *J. Am. Chem. Soc.* **2013,** *135*, 862-869.

32. Lee, C. Y.; Farha, O. K.; Hong, B. J.; Sarjeant, A. A.; Nguyen, S. T.; Hupp, J. T., Light-Harvesting Metal–Organic Frameworks (MOFs): Efficient Strut-to-Strut Energy Transfer in Bodipy and Porphyrin-Based MOFs. *J. Am. Chem. Soc.* **2011,** *133*, 15858-15861.

33. Goswami, S.; Ma, L.; Martinson, A. B. F.; Wasielewski, M. R.; Farha, O. K.; Hupp, J. T., Toward Metal–Organic Framework-Based Solar Cells: Enhancing Directional Exciton Transport by Collapsing Three-Dimensional Film Structures. *ACS Appl. Mater. Interfaces* **2016,** *8*, 30863-30870.

34. Goswami, S.; Chen, M.; Wasielewski, M. R.; Farha, O. K.; Hupp, J. T., Boosting Transport Distances for Molecular Excitons within Photoexcited Metal–Organic Framework Films. *ACS Appl. Mater. Interfaces* **2018,** *10*, 34409-34417.

35. Park, J.; Jiang, Q.; Feng, D.; Zhou, H.-C., Controlled Generation of Singlet Oxygen in Living Cells with Tunable Ratios of the Photochromic Switch in Metal–Organic Frameworks. *Angew. Chem. Int. Edit.* **2016,** *55*, 7188-7193.

36. Sundström, V.; Pullerits, T., Photosynthetic Light-Harvesting: Reconciling Dynamics and Structure of Purple Bacterial LH2 Reveals Function of Photosynthetic Unit. *J. Phys. Chem. B* **1999,** *103*, 2327-2346.

37. Krueger, B. P.; Scholes, G. D.; Fleming, G. R., Calculation of Couplings and Energy-Transfer Pathways between the Pigments of LH2 by the ab Initio Transition Density Cube Method. *J. Phys. Chem. B* **1998,** *102*, 5378-5386.

38. Förster, T., Energiewanderung und Fluoreszenz. *Naturwissenschaften* **1946,** *33*, 166-175.

39. Duncan, T. V.; Frail, P. R.; Miloradovic, I. R.; Therien, M. J., Excitation of Highly Conjugated (Porphinato)palladium(II) and (Porphinato)platinum(II) Oligomers Produces Long-Lived, Triplet States at Unit Quantum Yield That Absorb Strongly over Broad Spectral Domains of the NIR. *J. Phys. Chem. B* **2010,** *114*, 14696-14702.

40. Wang, B.; Yang, Q.; Guo, C.; Sun, Y.; Xie, L.-H.; Li, J.-R., Stable Zr(IV)-Based Metal–Organic Frameworks with Predesigned Functionalized Ligands for Highly Selective Detection of Fe(III) Ions in Water. *ACS Appl. Mater. Interfaces* **2017,** *9*, 10286-10295.

41. Li, X.; Yu, J.; Gosztola, D. J.; Fry, H. C.; Deria, P., Wavelength-Dependent Energy and Charge Transfer in MOF: A Step toward Artificial Porous Light-Harvesting System. *J. Am. Chem. Soc.* **2019,** *141*, 16849-16857.

42. Anderson, R.; Gómez-Gualdrón, D. A., Increasing topological diversity during computational "synthesis" of porous crystals: how and why. *CrystEngComm* **2019,** *21*, 1653-1665.

43. Colón, Y. J.; Gómez-Gualdrón, D. A.; Snurr, R. Q., Topologically Guided, Automated Construction of Metal–Organic Frameworks and Their Evaluation for Energy-Related Applications. *Cryst. Growth Des.* **2017,** *17*, 5801-5810.

44. Rappe, A. K.; Casewit, C. J.; Colwell, K. S.; Goddard, W. A.; Skiff, W. M., UFF, a full periodic table force field for molecular mechanics and molecular dynamics simulations. *J. Am. Chem. Soc.* **1992,** *114*, 10024-10035.

45. Dassault Systèmes BIOVIA, Materials Studio, 6.0, San Diego: Dassault Systèmes, 2018

46. Shi, T.; Wang, P., GPView: A program for wave function analysis and visualization. *J. Mol. Graph. Modell.* **2016,** *70*, 305-314.

47. Gouterman, M., Spectra of Porphyrins. *J. Mol. Spectrosc.* **1961,** *6*, 138-163.

48. Marder, S. R.; Gorman, C. B.; Meyers, F.; Perry, J. W.; Bourhill, G.; Brédas, J.-L.; Pierce, B. M., A Unified Description of Linear and Nonlinear Polarization in Organic Polymethine Dyes. *Science* **1994,** *265*, 632-635.

49. Tretiak, S.; Chernyak, V.; Mukamel, S., Chemical Bonding and Size Scaling of Nonlinear Polarizabilities of Conjugated Polymers. *Phys. Rev. Lett.* **1996,** *77*, 4656-4659.

50. Angiolillo, P. J.; Uyeda, H. T.; Duncan, T. V.; Therien, M. J., Impact of Electronic Asymmetry on Photoexcited Triplet-State

Spin Distributions in Conjugated Porphyrin Oligomers Probed via EPR Spectroscopy. *J. Phys. Chem. B* **2004,** *108*, 11893-11903.

51. Duncan, T. V.; Susumu, K.; Sinks, L. E.; Therien, M. J., Exceptional Near-Infrared Fluorescence Quantum Yields and Excited-State Absorptivity of Highly Conjugated Porphyrin Arrays. *J. Am. Chem. Soc.* **2006,** *128*, 9000-9001.

52. Zhang, T.-G.; Zhao, Y.; Asselberghs, I.; Persoons, A.; Clays, K.; Therien, M. J., Design, Synthesis, Linear, and Nonlinear Optical Properties of Conjugated (Porphinato)zinc(II)-Based Donor−Acceptor Chromophores Featuring Nitrothiophenyl and Nitrooligothiophenyl Electron-Accepting Moieties. *J. Am. Chem. Soc.* **2005,** *127*, 9710-9720.

53. Lovett, J. E.; Hoffmann, M.; Cnossen, A.; Shutter, A. T. J.; Hogben, H. J.; Warren, J. E.; Pascu, S. I.; Kay, C. W. M.; Timmel, C. R.; Anderson, H. L., Probing Flexibility in Porphyrin-Based Molecular Wires Using Double Electron Electron Resonance. *J. Am. Chem. Soc.* **2009,** *131*, 13852-13859.

54. Susumu, K.; Therien, M. J., Decoupling Optical and Potentiometric Band Gaps in π-Conjugated Materials. *J. Am. Chem. Soc.* **2002,** *124*, 8550-8552.

55. Deria, P.; Gómez-Gualdrón, D. A.; Bury, W.; Schaef, H. T.; Wang, T. C.; Thallapally, P. K.; Sarjeant, A. A.; Snurr, R. Q.; Hupp, J. T.; Farha, O. K., Ultraporous, Water Stable, and Breathing Zirconium-Based Metal–Organic Frameworks with ftw Topology. *J. Am. Chem. Soc.* **2015,** *137*, 13183-13190.

56. The corresponding modelling, however, were done without any solvent molecule present within the framework pores, which accounts for slight discripancies in the intensity matching.

57. Spek, A., Structure validation in chemical crystallography. *Acta Cryst. D.* **2009,** *65*, 148-155.

58. Prepared by solvent exchange, not through refilling of a dried sample.

59. Nasalevich, M. A.; Hendon, C. H.; Santaclara, J. G.; Svane, K.; van der Linden, B.; Veber, S. L.; Fedin, M. V.; Houtepen, A. J.; van der Veen, M. A.; Kapteijn, F.; Walsh, A.; Gascon, J., Electronic origins of photocatalytic activity in d^0 metal organic frameworks. *Sci. Rep.* **2016,** *6*, 23676.

60. Wu, X.-P.; Gagliardi, L.; Truhlar, D. G., Cerium Metal–Organic Framework for Photocatalysis. *J. Am. Chem. Soc.* **2018,** *140*, 7904-7912.

61. Tretiak, S.; Middleton, C.; Chernyak, V.; Mukamel, S., Exciton Hamiltonian for the Bacteriochlorophyll System in the LH2 Antenna Complex of Purple Bacteria. *J. Phys. Chem. B* **2000,** *104*, 4519-4528.

62. Mukamel, S.; Tretiak, S.; Wagersreiter, T.; Chernyak, V., Electronic Coherence and Collective Optical Excitations of Conjugated Molecules. *Science* **1997,** *277*, 781-787.

63. Karafyllidis, I. G., Quantum transport in the FMO photosynthetic light-harvesting complex. *J. Biol. Phys.* **2017,** *43*, 239-245.

64. The light intensity below few layers will be insignificant considering the hundreds of millimolar concentration for highly absorptive linker.

65. Lakowicz, J. R., Quenching of Fluorescence. In *Principles of Fluorescence Spectroscopy*, Lakowicz, J. R., Ed. Springer US: Boston, MA, 1983; pp 257-301.

66. Among the various well established quenching mechanisms static quenching causes only diminished QY, but does not display any linfetime quenching, whereas a dynamic quenching causes both.

67. Linkers did not show any detectable solvent dependency. DMF was consistently used for high solubility.

68. *i.e.* a c-polarized oscillator exciting another c-polarized oscilla-tor of its neighboring chromophore *via* emission-absorption with good OI.

69. Van Wyk, A.; Smith, T.; Park, J.; Deria, P., Charge-Transfer within Zr-Based Metal–Organic Framework: The Role of Polar Node. *J. Am. Chem. Soc.* **2018,** *140*, 2756-2760.

70. Yu, J.; Wyk, A. V.; Smith, T.; Deria, P., Charge Transfer within Metal-Organic Frameworks: The Role of Polar Node in the Electrocatalysis and Charge Storage. *ECS Trans.* **2018,** *85*, 559-564.

71. Hod, I.; Bury, W.; Gardner, D. M.; Deria, P.; Roznyatovskiy, V.; Wasielewski, M. R.; Farha, O. K.; Hupp, J. T., Bias-Switchable Permselectivity and Redox Catalytic Activity of a Ferrocene-Functionalized, Thin-Film Metal–Organic Framework Compound. *J. Phys. Chem. Lett.* **2015,** *6*, 586-591.

Insert Table of Contents artwork here